World Electric Vehicle Journal

MDPI

Article

Advancing Dual-Active-Bridge DC–DC Converters with a New Control Strategy Based on a Double Integral Super Twisting Sliding Mode Control

Irfan Sami [1], Waleed Alhosaini [2,*], Danish Khan [3] and Emad M. Ahmed [2]

[1] Research & Development Department, Milim Syscon Co., Ltd., Seongnam-si 13647, Republic of Korea; irfansamimwt@gmail.com
[2] Department of Electrical Engineering, College of Engineering, Jouf University, Sakaka 72388, Saudi Arabia; emamahmoud@ju.edu.sa
[3] Department of Electrical Engineering, Zhejiang University, Hangzhou 310027, China; danishkhandirvi@zju.edu.cn
* Correspondence: wsalhosaini@ju.edu.sa

Abstract: Dual-Active-Bridge (DAB) DC–DC converters are becoming increasingly favored for their efficiency in transferring electrical power across varying voltage levels. They are crucial in enhancing safety and reliability in various fields, such as renewable energy systems, electric vehicles, and the power supplies of electronic devices. This paper introduces a new control strategy for bidirectional isolated DAB DC–DC converters, implementing a Double Integral Super Twisting Sliding Mode Control (DI-STSMC) to accurately regulate the output voltage and current. The approach starts with a state-space representation to mathematically model the DAB converter. In light of model uncertainties and external disturbances, a robust DI-STSMC controller has been formulated to optimize the DAB converter's output performance. This method achieves zero steady-state error without chattering and provides a quick response to fluctuations in load and reference changes. The validity of the proposed technique is demonstrated through simulation results and a control hardware-in-the-loop (CHIL) experimental setup, using Typhoon HIL 606 and Imperix B-Box RCP 3.0 on a 230 W DAB converter. Furthermore, the paper offers a comparative analysis of the DI-STSMC with other control strategies, such as the proportional-integral (PI) controller, standard sliding mode control (SMC), and integral sliding mode control (ISMC).

Keywords: dual-active-bridge (DAB); DC–DC converters; sliding mode control (SMC); super twisting SMC (STSMC)

Citation: Sami, I.; Alhosaini, W.; Khan, D.; Ahmed, E.M. Advancing Dual-Active-Bridge DC–DC Converters with a New Control Strategy Based on a Double Integral Super Twisting Sliding Mode Control. *World Electr. Veh. J.* **2024**, *15*, 348. https://doi.org/10.3390/wevj15080348

Academic Editor: Yujie Wang

Received: 26 June 2024
Revised: 20 July 2024
Accepted: 26 July 2024
Published: 1 August 2024

1. Introduction

The Dual-Active-Bridge (DAB) and CLLC converters are two well-known bidirectional converter topologies that have different features that make them suitable for different applications. Because of their effective power transfer methods and minimal conduction losses, DAB converters are well known for their high efficiency, which frequently surpasses 98%. Their precise control mechanisms and robust bidirectional power flow capability make them ideal for high-power applications like renewable energy systems and grid-tied inverters. On the other hand, CLLC converters, which use resonant operation to reduce switching losses and improve performance in medium-power applications such as battery chargers and electric car charging stations, offer efficiency typically ranging from 95% to 98%. However, the control complexity of CLLC converters is higher, necessitating the use of complicated control techniques to successfully govern the dynamics of the resonant tank. This comparative analysis offers insights into choosing the best converter architecture based on efficiency, control complexity, and application requirements. It is influenced by current methodology and findings from reliable sources [1]. A detailed study of converter for electric vehicles can be found in [2]. Resonant converter topologies for

electric vehicle (EV) chargers are thoroughly reviewed in this work, with an emphasis on specific classification and selection criteria according to power rating and power flow requirements. The modulation and control strategies of high-efficiency LLC type resonant converters, as well as their use in vehicle-to-grid (V2G) operations, are the subjects of particular study [2,3]. The DAB DC–DC converter is gaining significant attention due to its efficient power transfer capabilities, reduced need for passive components, high power density, and excellent efficiency achieved through zero voltage switching (ZVS). It also features a high voltage conversion ratio and provides galvanic isolation. Crucially, it acts as an integral link between supercapacitors and batteries within energy storage systems (ESSs), enabling seamless energy management between ESSs and DC microgrids [4–6].

Numerous studies have explored various phase shift modulation techniques for DAB converters, such as the single phase shift (SPS) [7], extended phase shift (EPS) [8–10], double phase shift (DPS) [11–13], and triple phase shift (TPS) [14]. SPS, being the simplest, offers limited control over the converter, but suffers from constrained ZVS zones, heightened current stress, and back flow power, leading to suboptimal performance in low power settings [15,16]. In contrast, EPS modulation enhances the ZVS range and reduces both back flow power and current stress in medium power applications, using one bridge to adjust the inner phase shift ratio while both inner and outer ratios control the converter. DPS modulation expands this by introducing an additional control input, and TPS modulation further extends control options with two alternate inner phase shift ratios for the H-bridges and an additional outer phase shift, although it presents a more complex control scenario [17].

Efforts to boost the efficiency and dynamic capabilities of DAB converters under various modulation schemes are ongoing, with a focus on optimizing back flow power and current stress. For instance, a method to enhance these aspects under EPS control is described in [18]. However, this method relies on offline calculations, and is sensitive to disturbances. Separate offline strategies have been developed to adjust phase shift ratios without optimizing both back flow power and current stress simultaneously [19,20]. Modern approaches include online optimization (ONO) techniques that adjust phase shift ratios dynamically, improving efficiency without requiring detailed power stage calculations [14,21–23]. A unified phase shift control for ONO is outlined in [14], and a two-dimensional optimization using a simplex optimizer is proposed in [21]. A hybrid approach using TPS with ONO to enhance current stress and ZVS is discussed in [22], while [23] introduces a neural network-based TPS modulation and a fuzzy inference system for ONO.

Moreover, while proportional-Integral-Derivative (PID) controllers are widely used for their steady state control capabilities, their performance can falter under dynamic conditions due to the DAB converter's nonlinear characteristics [24,25]. Various control techniques, such as feedforward plus feedback, linearization, disturbance-observer-based control (DOBC), sliding mode control (SMC), and model predictive control (MPC), are employed to manage and enhance the performance of the DAB converter [26]. A comparative analysis of these methods demonstrates their effectiveness in maintaining output voltage stability amid load fluctuations [27]. Advances include a nonlinear MPC with phase-shift ratio compensation to boost dynamic response [28] and strategies that combine TPS modulation with advanced methods like the augmented Lagrangian method for reactive power reduction and improved soft switching [29].

The inherent robustness of SMC, along with its simplicity and adaptability, makes it ideal for controlling nonlinear systems like the DAB converter under uncertain conditions [25,30–34]. To reduce the typical chattering associated with SMC, integral SMC (ISMC) and double ISMC (DI-SMC) techniques have been developed. The super-twisting SMC (STSMC) approach, notable for its reduced chattering and finite time response, although lacking in some robustness aspects of traditional SMC, is further refined in this study [35]. We propose a double integral STSMC (DI-STSMC) scheme that incorporates DISMC and STSMC, aiming to minimize chattering and adapt to external disturbances and parameter variations. This new scheme has been rigorously tested in simulations and a CHIL setup with the Imperix B-Box (RCP 3.0) controller and Typhoon HIL 606, demonstrating superior

performance with fast convergence and minimal chattering compared to existing methods. The major contributions of this work are given as follows:

- This work presents a new DI-STSMC technology aimed at improving power electronic converter control performance in EV chargers. We have shown, by thorough Lyapunov stability analysis, that the proposed DI-STSMC guarantees zero steady-state error, offering strong system stability without requiring the conventional Bode analysis that is usually used for linear systems. This breakthrough in methodology establishes a new benchmark for preserving exact control in intricate, nonlinear systems.
- Comparing the DI-STSMC methodology to conventional SMC and ISMC techniques, our research demonstrates a considerable improvement in ripple performance. The robustness of the DI-STSMC under various load situations and step changes in reference voltage is validated by thorough simulations and Hardware-in-the-Loop (HIL) evaluations, underscoring its usefulness in preserving stability and optimum performance in real-world scenarios. These validations attest to the DI-STSMC methodology's applicability and dependability for EV charging applications.
- This work utilizes Typhoon HIL for plant simulations and the Imperix controller for the practical operation of DI-STSMC, which offers a useful framework that highlights the viability of our methodology. While in-depth loss evaluations were not the focus of this study, we describe future work that will integrate loss modeling and thorough analysis to further improve the usefulness of the DI-STSMC technique. This research contributes to theoretical understanding and offers useful direction for the design and implementation of sophisticated control systems in EV chargers by providing these in-depth insights and recommendations.

2. Modeling of DAB Converter

The DAB converter's output voltage at the HV bridge is characterized by a low harmonic model, as presented in [36]. The fundamental switching function represents a square wave, which is stated as follows:

$$\mathfrak{S}_A = \frac{1}{2} + \frac{2}{\pi}\sum_{k=0}^{\infty}\frac{1}{2k+1}\sin((2k+1)(ft) \tag{1}$$

The primary side voltage can be determined as follows:

$$v_{\mathrm{p}} = V_{\mathrm{in}}\left\{\frac{4}{\pi}\sum_{k=0}^{\infty}\frac{1}{2k+1}\sin((2k+1)(ft)\right\} \tag{2}$$

Similarly, with HV bridges and MOSFETs, the switching phenomenon is stated as follows:

$$\begin{aligned} v_{\mathrm{s}} &= v_{\mathrm{o}}[\mathfrak{S}_B - \mathfrak{S}_B] \\ v_{\mathrm{s}} &= v_{\mathrm{o}}\left\{\frac{4}{\pi}\sum_{k=0}^{\infty}\frac{1}{2k+1}\sin((2k+1)(ft-\delta))\right\} \end{aligned} \tag{3}$$

where δ represents the phase shift of the modulation signal. In Figure 1, the HV bridge receives power, and the modulation approach for the secondary bridge involves a phase shift of δ compared to the primary bridge. Utilizing the fundamental Kirchhoff voltage laws (KVL) on the HV side results in the equation presented:

$$i_{Lk}(t)R_{Lk} + L_k\frac{d}{dt}i_{Lk} = Nv_{\mathrm{p}}(t) - v_{\mathrm{s}}(t) \tag{4}$$

where N represents transformer turns ratio, which is $Ns : Np$. By combining (2), (3), and (4), the inductor current and impedance are:

$$i_{Lk}(t) = \frac{4}{\pi}\sum_{k=0}^{\infty}\frac{1}{(2k+1)}\left[\frac{Nv_p}{|\mathcal{Z}(k)|}\sin[(2k+1)ft] - \Psi_{\mathcal{Z}}(k) - \frac{v_s}{|\mathcal{Z}(k)|}\sin[(2n+1)(ft-\delta)] - \Psi_{\mathcal{Z}}(k)\right] \tag{5}$$

where

$$|\mathcal{Z}(k)| = \sqrt{R_{Lk}^2 + [(2k+1)\omega_s L_k]^2}$$
$$\varphi_{\mathcal{Z}}(k) = \tan^{-1}\left(\frac{(2k+1)\omega_s L_k}{R_{Lk}}\right) \tag{6}$$

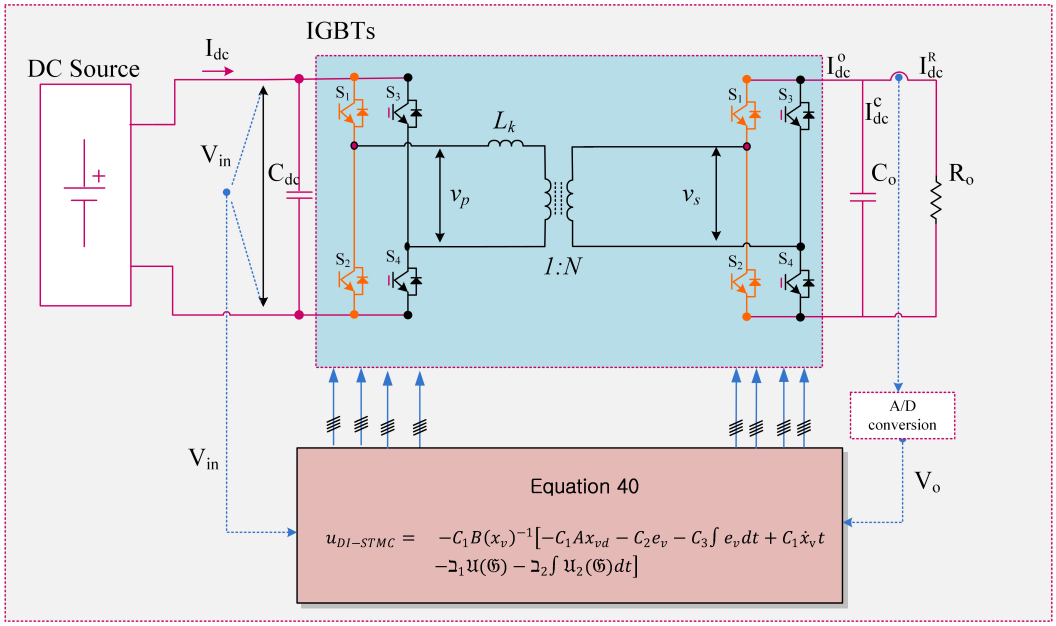

Figure 1. Control block diagram of Dual-Active-Bridge-based DC–DC converter.

$\mathcal{Z}(k)\angle\Psi_z(k)$ represents the impedance magnitude and its angle. Applying the Kirchhoff current (KCL) law on the converter HV side gives:

$$C_o\frac{dv^o_{dc}}{dt} = i^o_{dc} - i^R_{dc} \tag{7}$$

The output current i_{out} can be expressed using the switching states and the inductor current, specifically $i_{out} = i_{Lk}(S_B - S^*_B)$. Integrating (7) with the formula for the inductor current, and incorporating (3) and (5) into the resulting equation, yields the following formula:

$$\frac{d}{dt}v_o = -\frac{v_o(t)}{R_L} + \frac{1}{C_o}\left[\frac{Nv_{in}}{(2k+1)|\mathcal{Z}(k)|}\frac{4}{\pi}\sum_{k=0}^{m}(2k+1)f_s t - \Psi_{\ddagger}(k)\right] - v_{dc}\sin((2k+1)f_s t - \delta - \Psi_z(k))] + \frac{4}{\pi}\sum_{p=0}^{1}\frac{1}{(2p+1)}\sin((2p+1)(f_s t - \delta)) \tag{8}$$

The output voltage's final expression may be found by simplifying (8) as follows:

$$\frac{dv_o}{dt} = \frac{-8}{C_o\,\pi^2}\sum_{n=1,3,5,\ldots}^{\infty}\frac{v_o}{n^2|\mathcal{Z}(n)|}\cos(\Psi_z(n)) + \frac{8}{C_o\pi^2}\sum_{n=1,3,5,\ldots}^{\infty}\frac{Nv_{in}}{n^2|\mathcal{Z}(n)|}\cos(n\delta-\Psi_z(n)) - \frac{i_o}{C_o} \tag{9}$$

For the odd harmonic states, denoted by n = 1,3,5,… n = 1,3,5,…, Equation (9) illustrates the nonlinear relationship between the phase shift ($\delta\delta$) and voltage dynamics in the HV bridge. The state space representation corresponding to (9) is characterized as follows:

$$\dot{x}_v = \mathcal{A}(x_v) + \mathcal{B}(x_v)u + \mathcal{D} \tag{10}$$

The state matrices in this case are denoted by $A(x_v)$ and $B(x_v)$, where u is the control signal, which will be described in terms of a phase shift signal, and $x \in R^r$ represents the system's state. Furthermore, the following is the expression for the state matrices:

$$\begin{aligned}\mathcal{A}(x_v) &= \frac{-8}{C_o\,\pi^2}\sum_{n=1,3,5,\ldots}^{\infty}\frac{\cos(\Psi_z(n))}{n^2|\mathcal{Z}(n)|}v_o\\ \mathcal{B}(x_v) &= \frac{8}{C_o\,\pi^2}\sum_{n=1,3,5,\ldots}^{\infty}\frac{1}{n^2|\mathcal{Z}(n)|}Nv_{in}\\ \mathcal{D} &= -\frac{i_o}{C_o}.\end{aligned} \tag{11}$$

Given that the system attributes are expected to vary within a limited scope, both the uncertainties and parametric uncertainties can be incorporated into the disturbance term D to enhance its definition. The aggregated disturbance can thus be articulated as follows:

$$\mathcal{G} = \mathcal{D} + \Delta d_o + \Delta d_{in} + \Delta A(x_v) + \frac{8}{C_o\pi^2}\sum_{n=3,5,\ldots}^{\infty}\left[\frac{\cos(\varphi_z(n))}{n^2|\mathcal{Z}(n)|}v_o - \frac{1}{n^2|\mathcal{Z}(n)|}Nv_{in}\right] \tag{12}$$

where Δd_{source} and Δd_{load}, respectively, are used to represent the disturbances in source and load side, respectively. The uncertainty representation for the parameters is $\Delta A(x_v)$. Using the definitions given above, (12) may be stated as:

$$\dot{x}_v = \mathcal{A}(x_v) + \mathcal{B}(x_v)u + \mathcal{G} \tag{13}$$

Therefore, the DAB converter's nonlinear model is represented by (13).

3. Design of Controllers

SMC is a nonlinear control methodology that functions through a predefined sliding surface, which delineates the difference between the current and desired states of the system. The controller uses a control input to guide the system toward this surface. Due to its invariance in the sliding mode and robustness to uncertainties, SMC is recognized as a viable and efficient control system choice. It excels in managing unpredictable or dynamic system properties and disturbances, providing rapid and accurate responses to changes in system dynamics. Additionally, SMC is easier to develop and deploy than conventional linear control methods, often surpassing them under various conditions. This section will explore the development of multiple controllers, including SMC, Integral SMC (ISMC), Double Integral SMC (DI-SMC), and the innovative Double Integral Super-Twisting SMC (DI-STSMC).

3.1. Sliding Mode Control Design

The first step in the design of SMC is the definition of error. The equilibrium point is achieved using the error given as follows:

$$e_v = x_v - x_v^* \tag{14}$$

where the x_v is the actual state and x_v^* is the desired reference point. The rate of change of error in form of derivative is given as follows:

$$\dot{e}_v = \dot{x}_v - \dot{x}_v^* \tag{15}$$

The sliding surface is also selected as the error given in above equation, and is given as follows:

$$S_1 = e_v \tag{16}$$

The derivative of sliding surface with using the state space equation in (13) is given as follows:

$$\dot{S}_1 = \dot{e}_v = \mathcal{A}(x_v) - \mathcal{B}(x_v)u - \mathcal{G} - \dot{x}_v^* \tag{17}$$

The rate at which a state approaches the sliding surface can be enhanced by employing a reaching law, defined as follows:

$$u_{smc} = -\beta_1 |S_1| \quad \text{sign}\left(\frac{S_1}{\varrho_1}\right) \tag{18}$$

The final control is combination of equivalent control law U_{eq} and reaching law given in (18). Thus, the equivalent control law is achieved by taking $\dot{S}$ equal to zero to ensure that the sliding phase is achieved, and the final control law becomes [36]

$$u_{smc} = -B(x_v)^{-1}\left[\dot{x}_v^* - Ax_{vd} - \beta_1 |S_1| \quad \text{sign}\left(\frac{S_1}{\varrho_1}\right)\right] \tag{19}$$

Lyapunov Stability of SMC

Let us take the Lyapunov function $V = \frac{1}{2}S_1^T S_1$ and, taking its derivative, one obtains [37]

$$\dot{V} = S_1^T \dot{S}_1 \tag{20}$$

Putting the value of $\dot{e_v}$ from (17) in (20), one obtains

$$\dot{V} = S_1^T(\mathcal{A}(x_v) - \mathcal{B}(x_v)u_{smc} - \dot{x}_v^*) \tag{21}$$

$$\dot{V} = S_1^T(\mathcal{A}(x_v) - \mathcal{B}(x_v)(-B(x_v)^{-1}\left[\dot{x}_v^* - Ax_{vd} - \beta_1 |S_1| \quad \text{sign}\left(\frac{S_1}{\varrho_1}\right)\right]) - \dot{x}_v^*) \tag{22}$$

$$\dot{V} = S_1^T(-\beta_1 |S_1| \quad \text{sign}\left(\frac{S_1}{\varrho_1}\right)) \leq 0 \tag{23}$$

which is negative definite. The Lyapunov stability analysis ensures the system's asymptotic stability and finite time convergence. The SMC scheme for voltage regulation of DAB converter system meets these criteria.

3.2. Integral SMC

In this subsection, the ISMC is developed based on the nonlinear state space model outlined in (13). This controller is often employed in scenarios requiring high precision and strong robustness. Integrating an integral term within the controller's design aids in minimizing steady-state discrepancies in its response. To enhance the reduction of steady-state errors, the sliding surface is designed to include both historical and current error components, which are defined as follows:

$$\mathcal{S}_2 = \mathcal{C}_1 e_v + \mathcal{C}_2 \int e_v \tag{24}$$

In this instance, C_1 and C_2 are the gains associated with the sliding surface. Differentiation of (24) and its subsequent integration with (17) results in the equation below.

$$\dot{S}_2 = C_1(A(x_v) + B(x_v)u + G - \dot{x}_{vd}) + C_2 e_v \tag{25}$$

From (19), the control law becomes:

$$u_{ISMC} = -C_1 B(x_v)^{-1}\left[-C_1 A x_{vd} - C_2 e_v + C_1 \dot{x}_{vd} - \beta_2 |S_2| \quad \text{sign}\left(\frac{S_2}{\varrho_2}\right)\right] \tag{26}$$

The ISMC controller does not contain any integral terms, as shown in (26). Consequently, in steady-state circumstances, the steady-state error could occur.

Lyapunov Stability of Integral SMC

Let us take the Lyapunov function $V_2 = \frac{1}{2} S_2^T S_2$, and take its derivative

$$\dot{V}_2 = S_2^T \dot{S}_2 \tag{27}$$

Putting the value of $\dot{e_v}$ from (25) into (27) yields

$$\dot{V}_2 = S_2^T(C_1(A(x_v) + B(x_v)u + G - \dot{x}_{vd}) + C_2 e_v) \tag{28}$$

$$\begin{aligned}\dot{V}_2 = S_1^T\Big(\mathcal{A}(x_v) - \mathcal{B}(x_v)\Big[-C_1 B(x_v)^{-1}(-C_1 A x_{vd} - C_2 e_v \\ + C_1 \dot{x}_{vd} - \beta_2 |S_2|^q \,\text{sign}\left(\frac{S_2}{\varrho_2}\right)\Big]\Big) - \dot{x}_v^*\end{aligned} \tag{29}$$

$$\dot{V}_2 = S_1^T(-\beta_2 |S_2| \quad \text{sign}\left(\frac{S_2}{\varrho_3}\right)) \leq 0 \tag{30}$$

which is negatively definite. A Lyapunov stability examination verifies that the system achieves asymptotic stability and converges within a finite period. The SMC applied for voltage control in the DAB converter system meets these criteria.

3.3. Double Integral Sliding Mode Control Design

To achieve accurate convergence to the desired operating point, the DI-SMC is employed. This approach enhances control by integrating error terms twice into the sliding surfaces, effectively diminishing steady-state error and alleviating chattering. The error terms, characterized by double integral functions, are specified as follows:

$$\mathfrak{G} = S_v + C_3 \int \int e_v \tag{31}$$

Equation (31), referred as the reaching law, is the key element in designing control law. The derivative of (31) is obtained as follows:

$$\begin{aligned}\dot{\mathfrak{G}} = C_1(A(x_v) + B(x_v)u + G - \dot{x}_{vd}) \\ + C_2 e_v + C_3 \int e_v \, dt\end{aligned} \tag{32}$$

From (32), the final control law using the SMC based reaching law and equivalent control obtained by equalizing (31) to 0, becomes

$$\begin{aligned}u_{DI-SMC} = -C_1 B(x_v)^{-1}[-C_1 A x_{vd} - C_2 e_v \\ -C_3 \int e_v \, dt + C_1 \dot{x}_{vd} - \beta_3 |\mathfrak{G}| \,\text{sign}\left(\frac{\mathfrak{G}}{\varrho_3}\right)\Big]\end{aligned} \tag{33}$$

The DI-SMC improves the robustness of the the conventional SMC, whereas it also helps in minimizing chattering, but still the signum function in (33) results in a considerable chattering. Thus, to minimize the chattering while maintaining the inherent robustness of the SMC, a STSMC based control law will be introduced in the next section.

Lyapunov Stability of Double Integral SMC

Let us take the Lyapunov function $V_3 = \frac{1}{2}\mathfrak{G}^T\mathfrak{G}$ and take its derivative

$$\dot{V}_3 = \mathfrak{G}2^T\dot{\mathfrak{G}} \tag{34}$$

Putting the value of $\dot{e_v}$ from (32) into (34) yields

$$\dot{V}_3 = \mathfrak{G}^T(C_1(A(x_v) + B(x_v)u + G - \dot{x}_{vd}) + C_2e_v + C_3\int e_v) \tag{35}$$

$$\begin{aligned}\dot{V}_3 = \mathfrak{G}^T\Bigg(\mathcal{A}(x_v) - \mathcal{B}(x_v)\Bigg(-C_1B(x_v)^{-1}\Bigg[-C_1Ax_{vd} - C_2e_v - C_3\int e_v\,dt \\ +C_1\dot{x}_{vd} - \beta_3|\mathfrak{G}|^q\,\mathrm{sign}\left(\frac{\mathfrak{G}}{\varrho_3}\right)\Bigg]\Bigg) - \dot{x}_v^*\end{aligned} \tag{36}$$

$$\dot{V}_3 = \mathfrak{G}^T(-\beta_3|\mathfrak{G}| \quad \mathrm{sign}\left(\frac{\mathfrak{G}}{\varrho_3}\right)) \leq 0 \tag{37}$$

which is negative definite. The Lyapunov stability analysis ensures the system's asymptotic stability and finite time convergence. The DI-SMC scheme for voltage regulation of DAB converter system meets these criteria.

3.4. Design of Double Integral Super Twisting SMC

DI-STSMC, a modified version of SMC, reduces chattering through the use of higher-order derivatives and maintains strong resistance to external disturbances. This controller efficiently twists system trajectories back to the origin, ensuring rapid convergence with minimal chatter. The error terms, along with their time derivatives, were elaborated in the preceding section. The reaching law for DI-STSMC, designed to decrease chatter and enhance convergence to the sliding surface, is presented as follows:

$$\begin{aligned}\dot{\mathfrak{G}} &= \mathfrak{U}_1(\mathfrak{G}) + \mathfrak{h} \\ \dot{\mathfrak{h}} &= \mathfrak{U}_2(\mathfrak{G})\end{aligned} \tag{38}$$

The $\mathfrak{U}_1$ and $\mathfrak{U}_2$ are given as follows:

$$\begin{aligned}\mathfrak{U}_1 &= -\beth_1\sqrt{|\mathfrak{G}|}\,\mathrm{sign}\left(\frac{\mathfrak{G}}{\varrho_4}\right) \\ \mathfrak{U}_1 &= -\beth_2 \quad \mathrm{sign}(\mathfrak{G})\end{aligned} \tag{39}$$

where $\mathfrak{G} \in R^3, v \in R^3$, and $\beth_1, \beth_2$ are positive constants. Using the same surface given in (31) and reaching law given in (38), the final control law for DI-STSMC can be proposed as follows:

$$\begin{aligned}u_{DI-STMC} = -C_1B(x_v)^{-1}\Bigg[-C_1Ax_{vd} - C_2e_v - C_3\int e_v\,dt + C_1\dot{x}_{vd} \\ -\beth_1\mathfrak{U}(\mathfrak{G}) - \beth_2\int \mathfrak{U}_2(\mathfrak{G})\,dt\Bigg]\end{aligned} \tag{40}$$

Lyapunov Stability of Double Integral Supertwisting SMC

Let us take the Lyapunov function $V_4 = \frac{1}{2}\mathfrak{G}^T\mathfrak{G}$, and take its derivative

$$\dot{V}_4 = \mathfrak{G}2^T\dot{\mathfrak{G}} \tag{41}$$

Putting the value of $\dot{e_v}$ from (35) into (41) yields

$$\dot{V}_4 = \mathfrak{G}^T(C_1(A(x_v) + B(x_v)u_{DI-STSMC} + G - \dot{x}_{vd}) + C_2e_v + C_3\int e_v) \tag{42}$$

$$\dot{V}_4 = \mathfrak{G}^T\Big(\mathcal{A}(x_v) - \mathcal{B}(x_v)\Big(-C_1B(x_v)^{-1}\Big[-C_1Ax_{vd} - C_2e_v - C_3\int e_v\,dt + C_1\dot{x}_{vd} - \beth_1\mathfrak{U}(\mathfrak{G}) - \beth_2\int \mathfrak{U}_2(\mathfrak{G})\,dt\Big]\Big)\Big) \tag{43}$$

$$\dot{V}_4 = \mathfrak{G}^T(-\beth_1\mathfrak{U}(\mathfrak{G}) - \beth_2\int \mathfrak{U}_2(\mathfrak{G})) \leq 0 \tag{44}$$

which is negative definite. This demonstrates that the proposed controller is asymptotically stable and ensures voltage regulation within a finite time.

4. Results and Discussions

This section presents the simulation results carried out in Matlab/SIMULINK using the Imperix environment. A 230 Watt system with the parameters given in Table 1 is used to verify the controller performance. The plant quantities in the Imperix environment are modeled with continuous signals, which requires a variable-step solver to capture their dynamics accurately. The implementation of control algorithm is performed through the discrete signals that sampled at a equal rate to the interrupt frequency fully aligned with the phase of sampling performed throughout the simulations. The z-domain is necessary to discretize the signal during the simulations, which is accommodated by the variable-step solver taking major steps at each interrupt execution. Also, to represent the actual behavior of the real PWM generators, these simulations use the actual carrier-based PWM algorithms to generate the PWM signals. The duty-cycle and phase parameters are updated at specific instant the occurs at the maximum points and/or zero of the carrier wave signal. The duration of algorithm execution is also modeled, resulting in a delay between the commencement of the interrupt and the availability of the new data. By precisely modeling all delays and phases, the simulated controller has the same dynamics as the real controller, allowing for effective control parameter adjustment during offline simulations. The control parameters for the setup under investigation is given in Table 2.

Using the above simulation environment, this section provides the simulation results of various controllers including Proportional Integral (PI), SMC, ISMC, and DI-STMSC. The controllers are tested for various cases, which include: (a) change in reference voltage and (b) change in output voltage.

Table 1. Dual-Active-Bridge converter parameters for simulation and experimental setup.

Parameters	Value
Rated power	230 Watts
Input voltage V_{in}	50 V
Output voltage v_{o}	30 V to 60 V
f_s	20 Khz
C_{dc} , C_{o}	100 µF, 200 µF
Transformer,s turn ration	1
L_k	30 uH
Variable load (R_o)	1.1 × 10 watts

(PI) control, renowned for its simplicity and stability, showcases moderate overshoots and undershoots in DC link voltage regulation. The PI exhibits an overshoot of 3.5 V during the convergence to the reference voltage. Similarly, the output voltage takes 0.02 s to reach the reference voltage. The convergence and undershoot can also be experienced in the error, as shown in Figure 2a. The performance of PI controller during the sudden reference voltage is shown in Figure 2b. A undershoot of 10 in the error is given in Figure 2b. Under load variation, a PI controller exhibits an overshoot of approximately 3.5 V, owing to its integral action that tends to accumulate errors over time. Similarly, sudden load changes can prompt undershoots, with the voltage momentarily dipping by around 7V before stabilizing. The convergence to reference voltage is achieved in 0.02 s, as shown

in Figure 2c. The PI controller struggles to swiftly correct for load disturbances due to its reliance on error accumulation.

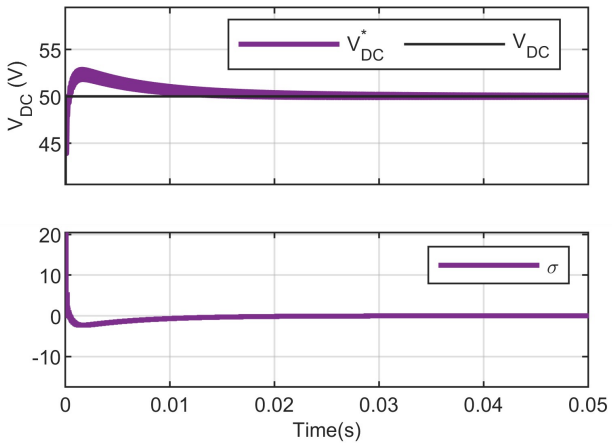

(**a**)

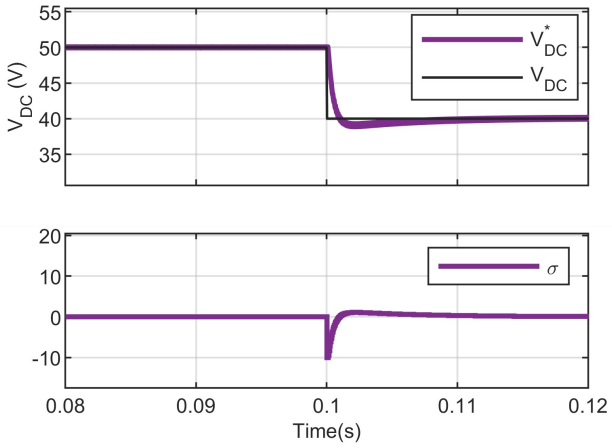

(**b**)

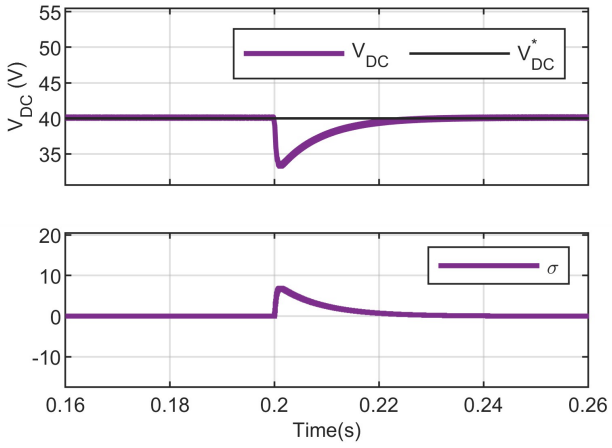

(**c**)

Figure 2. DC link voltage for PI (**a**) at starting time, (**b**) voltage reference variation, (**c**) during load change.

Table 2. Controller parameters and their numeric values.

Method	Parameters	Value
PI	K_p	8.514
	K_I	16
SMC	ϱ_1	0.8
	β_1	10
ISMC	ϱ_2	0.8
	β_2	12
	C_1	4
	C_2	2
DISMC	ϱ_3	6.328
	β_3	7
	C_3	3.567
DI-STSMC	$\lrcorner_1$	1.6
	$\lrcorner_2$	8
	ϱ_4	7.54

In contrast, SMC control scheme demonstrates enhanced performance, minimizing the convergence time and undershoots while ensuring a faster response to load variations, as shown in Figure 3. The starting performance of DAB operating under SMC is shown in Figure 3a. It can be seen that, with an approximate overshoot of 5 V and convergence time of of 0.003 s, SMC exhibits a robust capability to swiftly counteract disturbances. Its inherent sliding mode mechanism allows for precise voltage regulation, reducing the effects of both overshoots and undershoots. SMC utilizes a sliding surface predominantly based on a switching function, designed to ensure resilience against disturbances. The sliding surface in SMC operates on the principle of continuous switching to maintain control. During the voltage variation by decreasing the reference voltage by 10 V, the SMC offers overshoot of 2 V with a fast convergence time of 0.003 s, as shown in Figure 3b. This strategy notably minimizes undershoots during the load variation, resulting in an approximate 5 V undershoot and 0.003s convergence time. However, SMC exhibit chattering in due to its aggressive switching behavior. Overall, the sliding mode in SMC promptly respond to load variations by actively forcing the system towards the sliding surface, offering improved voltage regulation compared to PI controllers. Similarly, the response of SMC controller to the load variation is shown in Figure 3c. It can be seen that the undershoot in the voltage at t = 0.2 s is minimized, as compared to the PI controller scheme. The SMC offers undershoot of 6 V with an overshoot of 8 V in the state error. The convergence time is improved with a good extent. The SMC improves the overall performance, but it suffers with high chattering, as shown in the voltage and error profiles in Figure 3.

Moving to ISMC, this advanced control strategy further refines the voltage regulation process. The double integration of the sliding surface enables superior error compensation, resulting in reduced overshoots and undershoots. With a 0.001 s convergence time and an approximate overshoot of 3 V, ISMC has a strong ability to quickly reach the reference voltage, as shown in Figure 4a. Its built-in sliding mode mechanism reduces the impact of both overshoots and undershoots by precisely regulating the voltage. The ISMC provides undershoot of 1.4 V and a quick convergence time of 0.001 s during the voltage variation caused by lowering the reference voltage by 10 V, as shown in Figure 4b. This approach leads to an approximate 5 V undershoot and 0.002 s convergence time, significantly reducing undershoots and improving the convergence time throughout the load variation, as shown in Figure 4c. The ISMC lowers the chattering the a good extent, but the chattering is still not fully minimized.

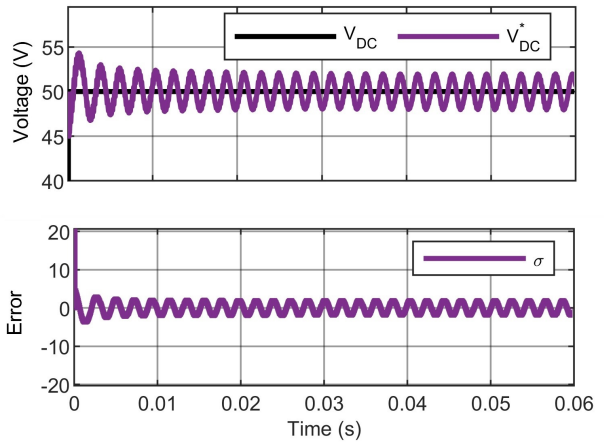

(**a**)

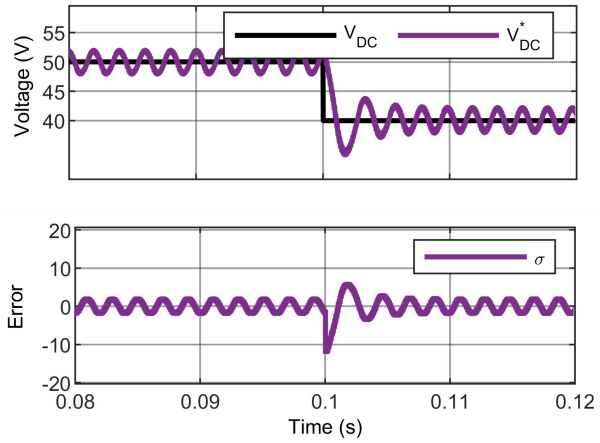

(**b**)

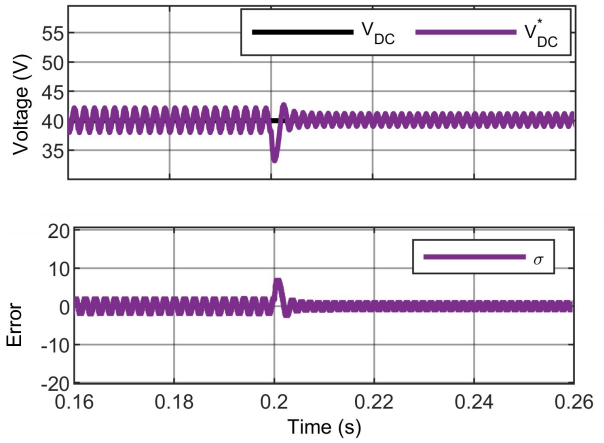

(**c**)

Figure 3. DC link voltage for SMC (**a**) at starting time, (**b**) voltage reference variation, (**c**) during load change.

Finally, the DI-STSMC takes voltage regulation to an even higher level of precision and stability. The proposed method keeps the robustness of the DI-SMC, whereas it minimized the overall chattering in the voltage profile. It can bee seen from Figure 5a that the proposed controller exhibits overshoot of 1.5 V with a very fast convergence time. The

convergence is also evident from the error profile in Figure 5a. Similarly, during voltage variation, the undershoot is negligible whereas the error profile is also improved, as shown in Figure 5b. With load fluctuations, this controller displays remarkable convergence behavior, with insignificant undershoot of around 3V and convergence time of 0.001s, as shown in Figure 5c. Super twisting algorithms let the controller to track the reference voltage quickly and precisely, exhibiting exceptional stability even in difficult situations. Superior performance in voltage regulation scenarios is ensured by the double integral super twisting SMC's complex control mechanism, which produces small deviations from the required voltage set-point.

The sliding surface's super twisting algorithms enable the controller to quickly and accurately push the system in the direction of the reference voltage, resulting in very little deviation and outstanding stability in voltage regulation situations. This controller is unique from others using SMC techniques because of its super twisting algorithms and complex sliding surface mechanism, which together provide higher precision and resilience in handling a range of operating circumstances while reducing chattering effects.

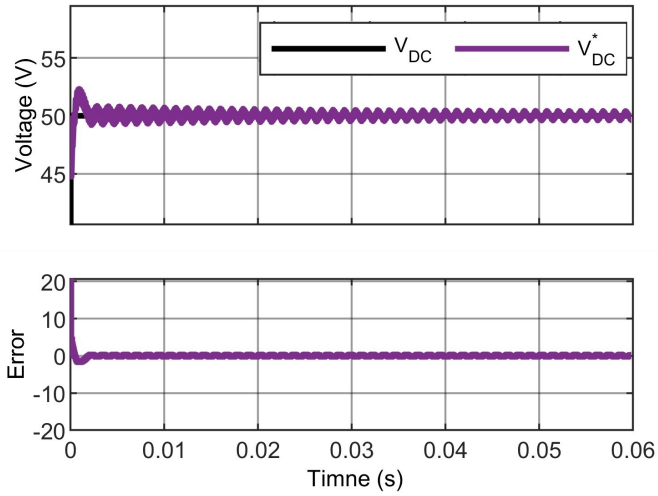

(**a**)

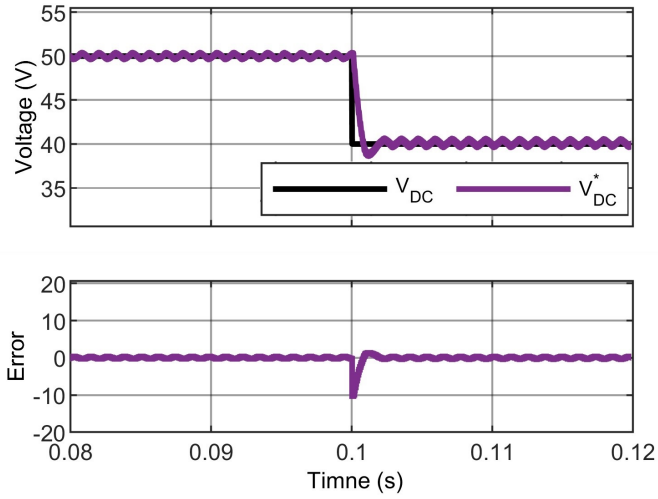

(**b**)

Figure 4. *Cont.*

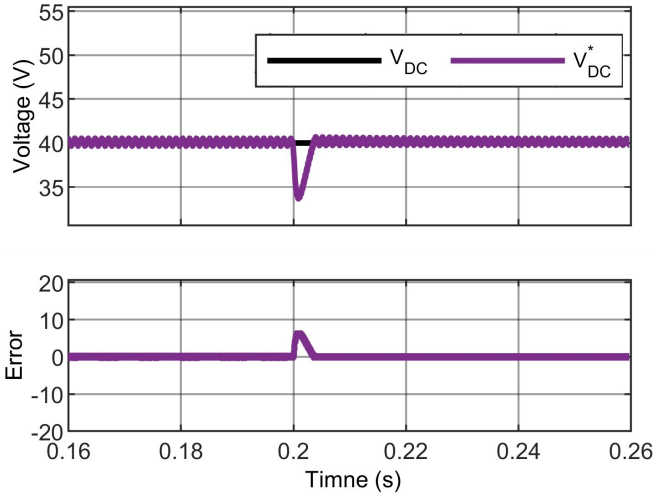

(**c**)

Figure 4. DC link voltage for ISMC (**a**) at starting time, (**b**) voltage reference variation, (**c**) during load change.

The effect of voltage and load variation on the primary voltage v_p and secondary voltage v_s is shown in Figure 6. The variation in voltage is experienced at t = 0.1 s, and variation in secondary voltage is experienced at t = 0.2 s. The v_p and v_s during PI operation in Figure 6a shows that the during voltage and load change; the PI acts very slowly to the disturbance and slow convergence to the actual value can be seen. During SMC operation in Figure 6b, a fast convergence can be seen, but variation due to high chattering is experienced in this case. The ISMC in Figure 6c helps in reducing the chattering while maintaining the inherent robustness, but could not eliminate the chattering. The proposed DI-STSMC in Figure 6d helps in eliminating the chattering while the double integral increases the robustness against the load and voltage variations and thus shows a very fast convergence after the disturbance happens to the actual values.

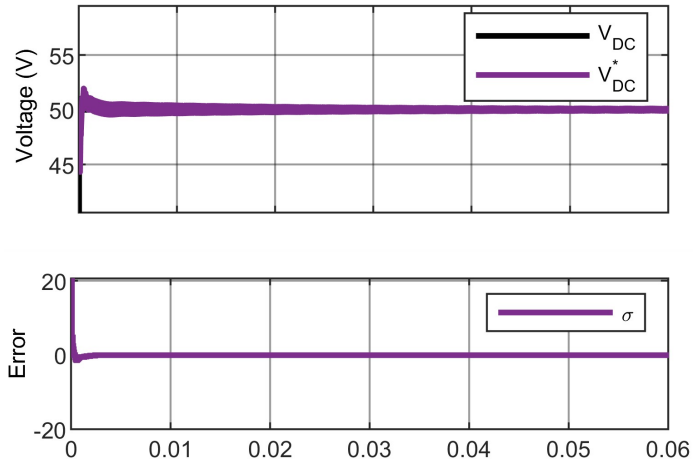

(**a**)

Figure 5. *Cont.*

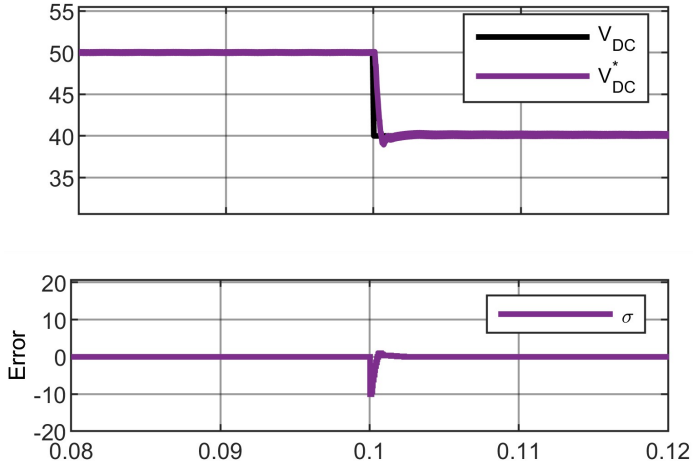

(**b**)

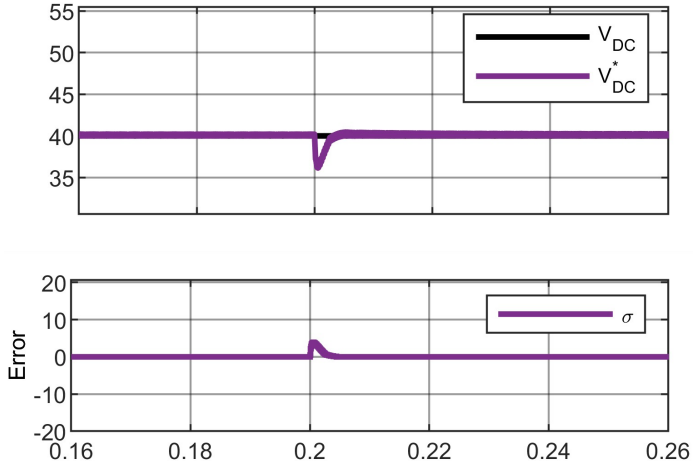

(**c**)

Figure 5. DC link voltage for proposed DI-STSMC control scheme (**a**) at starting time, (**b**) voltage reference variation, (**c**) during load change.

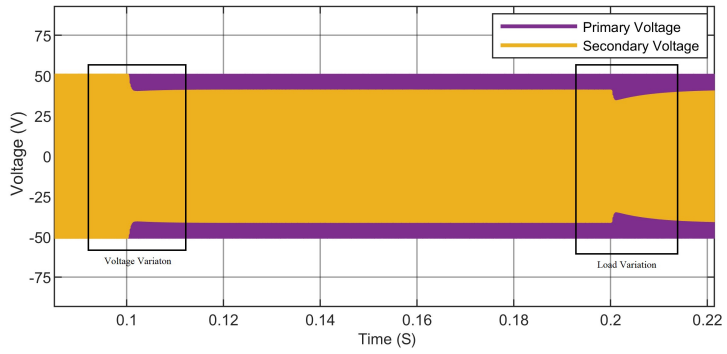

(**a**)

Figure 6. *Cont.*

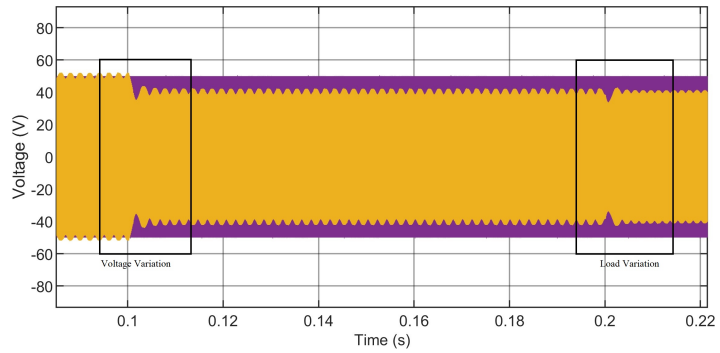

(**b**)

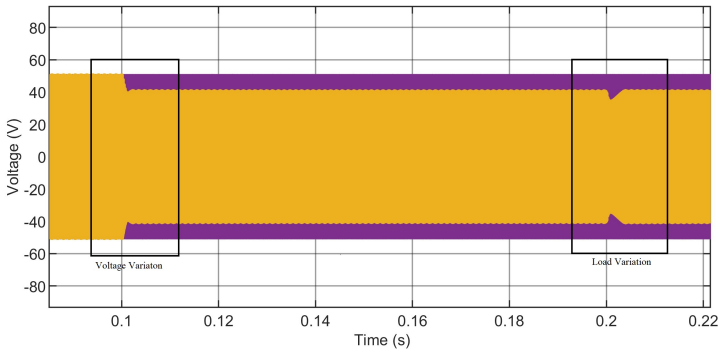

(**c**)

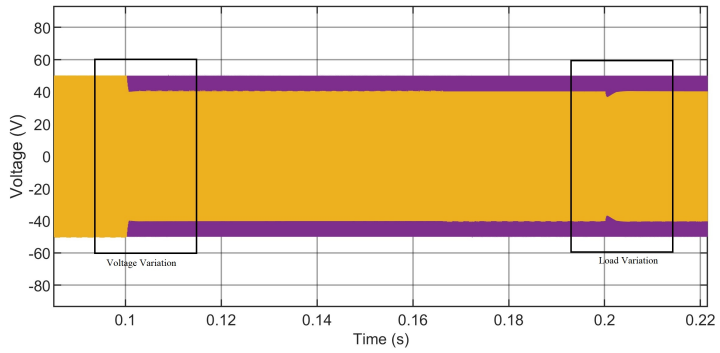

(**d**)

Figure 6. Primary and secondary voltage comparisons for voltage variations (**a**) PI, (**b**) SMC, (**c**) ISMC, (**d**) DI-STSMC.

5. Experimental Results

The behavior of the DAB system's voltage control is evaluated experimentally in both transient and steady-state conditions using control hardware in the loop (CHIL) system. The Imperix B-Box RCP-3.0 from Imperix Ltd., Sion, Switzerland and Typhoon HIL-606 from Typhoon HIL, Inc., Somerville, MA, USA are used in a CHIL configuration to carry out this control mechanism. Through the control unit, the Imperix B-Box RCP-3.0 is in charge of producing a pulse width modulation (PWM) signal that is then sent to HIL-606 to regulate the DAB converter. The link between the RCP-3.0 controller and the HIL-606 system is shown in Figure 7. In this configuration, the Typhoon schematic is used to model the hardware, and the controller's software is created in MATLAB/Simulink with the RCP-3.0 library. Typhoon SCADA is essential for examining hardware dynamics. The DAB primary voltage, secondary voltage, secondary current, and DC link voltage are shown in Figure 8. It can be seen from Figure 8a that the PI controller offers a high overshoot of 5 V and a slower convergence time of 1 s after the variation has happened. The overshoot in

the current and primary voltage is also evident from Figure 8a. Similarly, the SMC provides faster convergence and less overshoot during the voltage variation, but it exhibits high chattering. This chattering results in a bad current and voltage waveform that can be seen in Figure 8b. The convergence highly increases to 100 ms, resulting in increased chattering and deteriorated voltage and current waveforms. These variation in the voltage and current with high frequency chattering generally leads to high temperatures and thermal losses in the converter. The proposed DI-STSMC, when subjected to load variations, makes a smoother performance with good convergence time of 250 ms after the change in the reference voltage, as shown in Figure 8c. Also, the overshoot in the voltage waveform in minimal, leading to more smoother and chattering free voltage and current waveform.

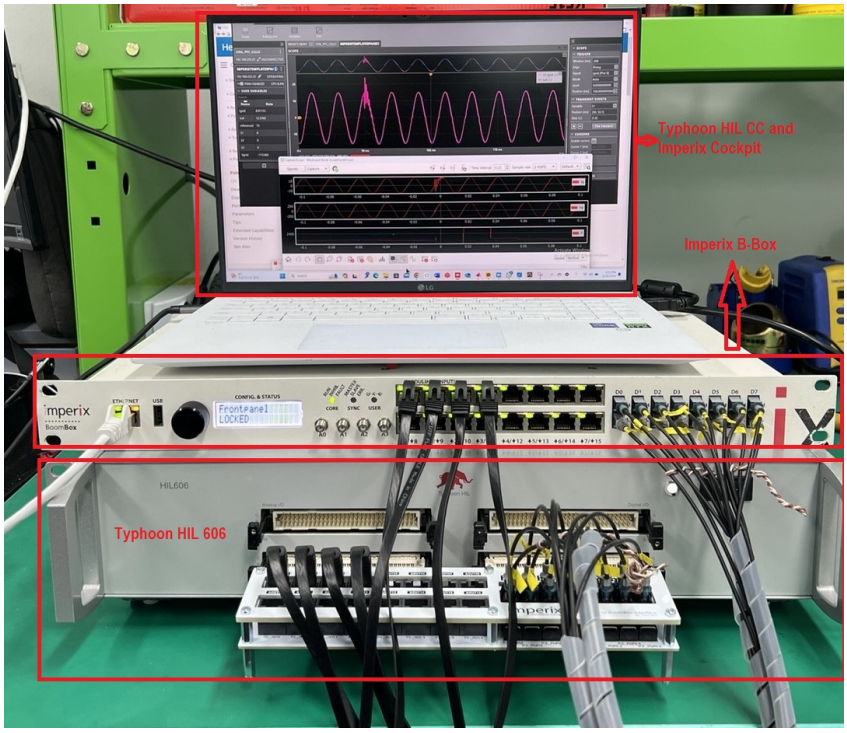

Figure 7. CHIL-based experimental system for proposed control scheme.

In the next test, the DAB converter is subjected to the load variation. Initially, a load is decreased and then increased by the same proportion. The response of the PI, SMC, and proposed DI-STSMC is shown in Figure 9. It can be seen from Figure 9a that the PI controller, relying on integral action, demonstrates high undershoot of 10 V during the decrease in the load and overshoot of approximately 12 V in response to the increase in the load. In contrast, SMC, known for its robustness in handling disturbances, displays reduced undershoots and overshoots at approximately 4 V and 4 V, respectively, as shown in Figure 9b. The convergence time to the actual value is also improved and it reaches to the actual value much faster as compared to the PI control scheme. The DI-STSMC, built for greater precision, is projected to produce minimum overshoots close to 5 V during both the rise and reduction of the DC link voltage, as given in Figure 9c. This demonstrates its outstanding stability and accuracy during rapid voltage changes. The chattering is eliminated in the voltage and current waveform, as shown in Figure 9c, whereas improving the overall stability against the variation in voltage and load.

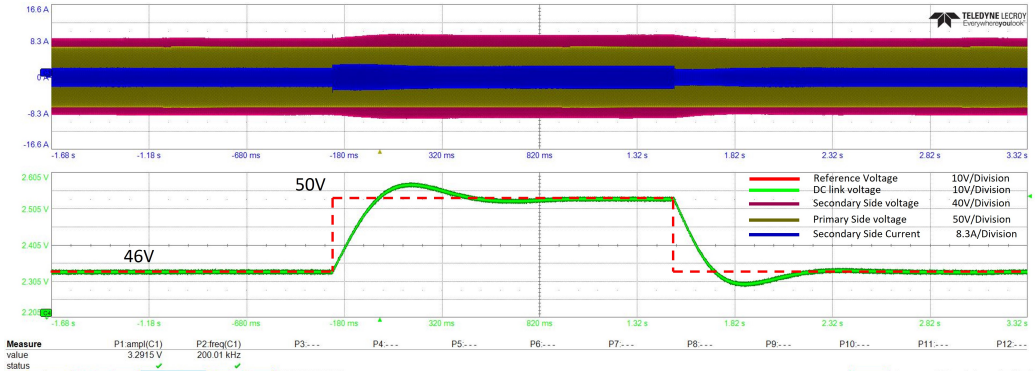

(**a**)

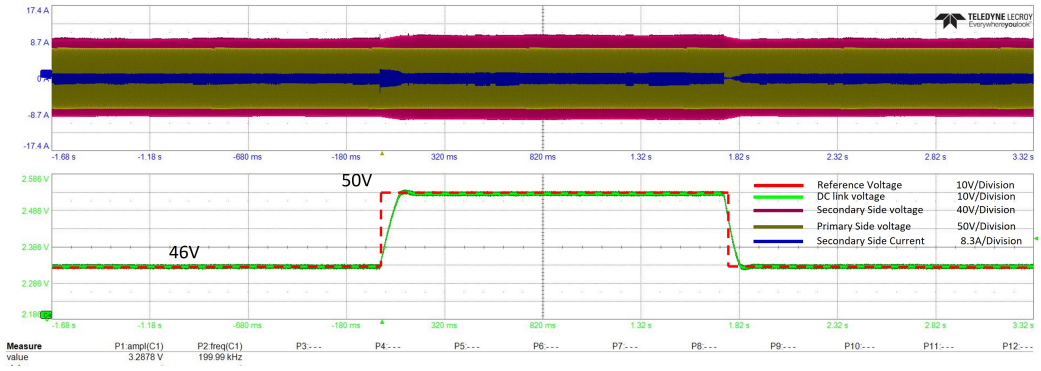

(**b**)

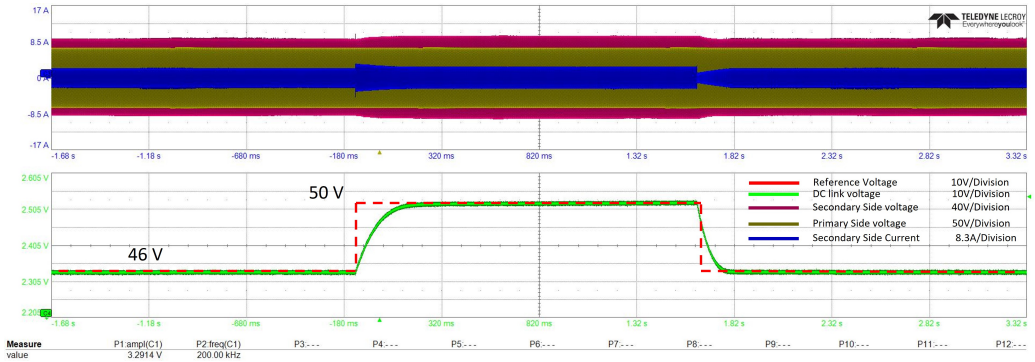

(**c**)

Figure 8. DC link voltage comparison for PI, SMC, and DI-STSMC at step input voltage change (**a**) PI, (**b**) SMC, (**c**) DI-STSMC.

These unique behaviors highlight each controller's differing capacities to regulate the DAB's output DC link voltage and currents under various load circumstances and during step changes in the DC link voltage. While the PI controller has moderate deviations due to its integral action, SMC has superior control with fewer deviations, but increased chattering, and the double integral super twisting SMC has exceptional precision, minimizing overshoots and undershoots in various operational scenarios, emphasizing their individual strengths in control and stability. We examined and compared the effectiveness of three control systems in our thorough examination of ripple factors: SMC, ISMC, and DI-STSMC. Under the same operating conditions, the ripple factor—which is the ratio of the peak-to-peak ripple voltage to the average output voltage—was evaluated. In our experiments, we found that SMC produced a 5.5% ripple factor, ISMC produced an enhanced 3.8% ripple factor, and our suggested DISTSMC approach further lowered the ripple factor to 2.2%. As an illustration of how well simulation studies matched experimental results, they projected ripple factors of 6.3% for SMC, 4.7% for ISMC, and 3.1% for DI-STSMC. The absence of some factors in the simulation model and idealized settings can be the cause of minor differences,

such as a slightly lower ripple factor in simulations. This comparison analysis confirms the resilience and efficacy of our suggested technique in both simulated and real-world scenarios by highlighting DI-STSMC's superior performance in minimizing ripple.

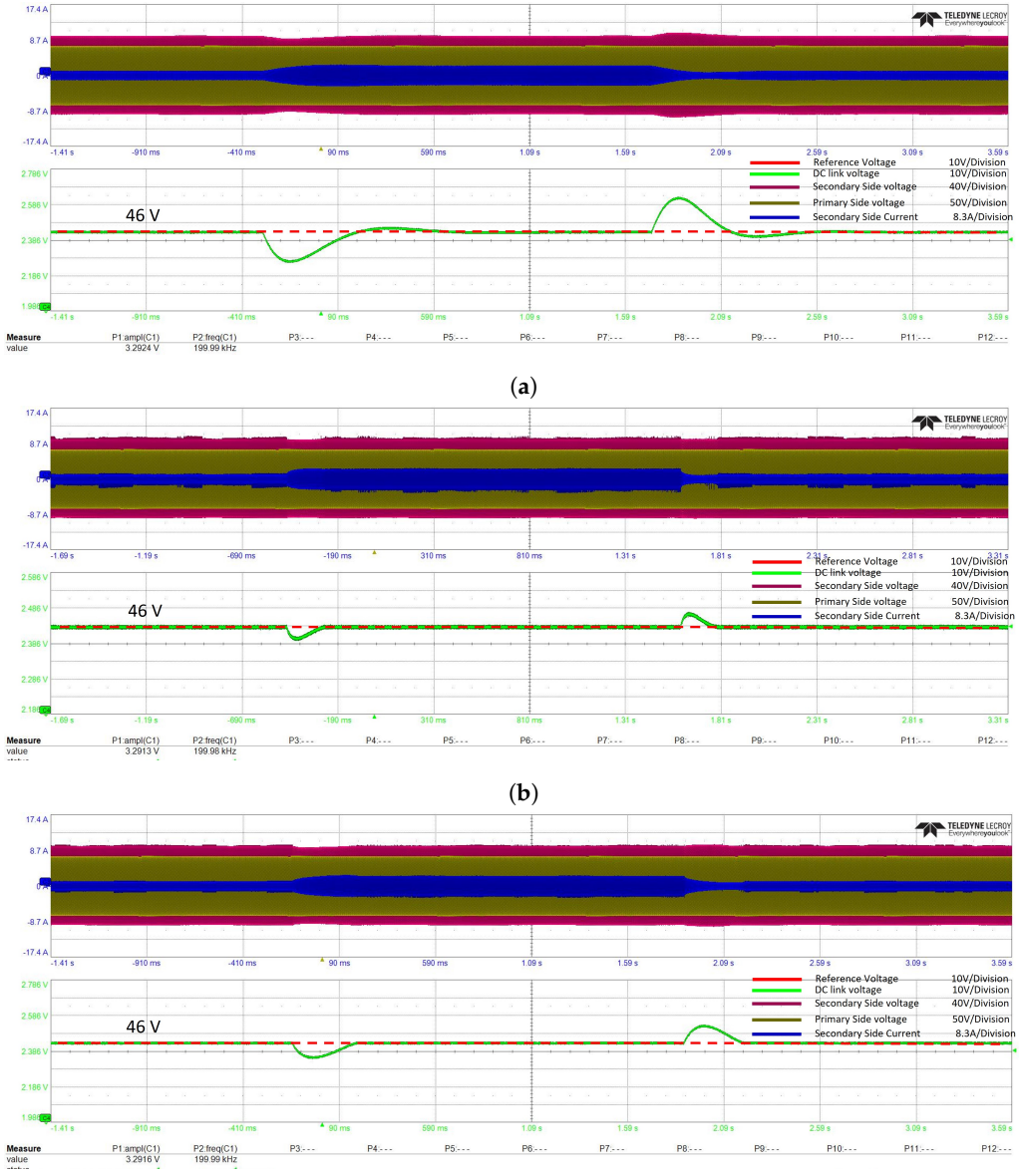

Figure 9. DC link voltage comparison for PI, SMC, and DI-STSMC during load variation (**a**) PI, (**b**) SMC, (**c**) DI-STSMC.

Practical Implementation and Limitations

There are various obstacles and factors to take into account when putting the DI-STSMC approach into practice. A prevalent problem is the chattering phenomena, which can be reduced by applying boundary layer methods or smooth switching function approximations. Robust terms in the control rule handle model uncertainties and disturbances, enabling dynamic adaptation to changing circumstances. High sampling rates and real-time processing are essential, thus sophisticated micro controllers or digital signal processors (DSPs) with effective algorithms must be used. High-accuracy sensors and capable mechanical components can be integrated to achieve precise control and robust disturbance rejection in mechanical systems, such as vehicle suspensions or robotic arms. Thermal control and the use of high-frequency switching devices are critical for electrical systems like motor drives and power

converters. Although the DI-STSMC approach provides strong nonlinear control and disturbance rejection, it is crucial to recognize that it may have certain disadvantages. These include the difficulty in creating an efficient sliding surface, the sensitivity to uncertainties in the system model, and the problem of minimizing chattering because of its discontinuous control input. Conventional control techniques, like PID control, may be advantageous in situations when seamless functioning and ease of design are critical. Based on the unique needs and characteristics of the application, careful consideration should be given to the decision between DI-STSMC and conventional approaches. The method's viability is demonstrated by running plant simulations with Typhoon HIL and implementing DI-STSMC on the Imperix controller. In order to further ensure dependable and efficient control in real-world applications, suitable hardware selection, strong software development, real-time operating systems (RTOS), and optimized code are required.

6. Conclusions

This study presents a DI-STSMC-based voltage control technique for DAB converters that provides better voltage regulation and robust control. Using DAB's average modeling simplifies controller design as compared to other non-linear converter controllers. The proposed DI-STSMC technique eliminates chattering in SMC, resulting in lower ripple in output voltage waveforms. Robust control is performed in the face of disruptions and uncertainties such as unanticipated load fluctuations and output voltage variations. The performance is verified by the numerical values of the output voltage; for instance, the proposed control gave minimum undershoot of 4 V followed by SMC and ISMC with 6 V and PI with highest undershoot of 7 V under load variation. The proposed control approach is experimentally tested and compared to SMC- and PI-based classical voltage control. The suggested control technique provides robust control with improved steady-state and transient performance, as demonstrated by experimental findings and comparisons. Improved tracking performance leads to higher steady-state output voltage, even with significant reference voltage changes.

Author Contributions: Conceptualization, I.S.; methodology, D.K.; software, W.A.; validation, I.S., E.M.A. and D.K.; formal analysis, I.S. and E.M.A.; investigation, X.X.; resources, W.A.; data curation, W.A.; writing—original draft preparation, I.S. and E.M.A.; writing—review and editing, I.S.; visualization, D.K.; supervision, I.S.; project administration, I.S.; funding acquisition, I.S. All authors have read and agreed to the published version of the manuscript.

Funding: The authors extend their appreciation to the Deputyship for Research & Innovation, the Ministry of Education in Saudi Arabia for funding this research work through project number 223202.

Institutional Review Board Statement: No humans or animal were involved in any experimental study.

Data Availability Statement: The original contributions presented in the study are included in the article; further inquiries can be directed to the corresponding author.

Acknowledgments: The authors are thankful to the Milim syscon.co, South Korea for providing experimental workbench for this study.

Conflicts of Interest: Irfan Sami was employed by the Milim Syscon Co., Ltd. The remaining authors declare that the research was conducted in the absence of any commercial or financial relationships that could be construed as a potential conflict of interest.

References

1. Min, J.; Ordonez, M. Bidirectional Resonant CLLC Charger for Wide Battery Voltage Range: Asymmetric Parameters Methodology. *IEEE Trans. Power Electron.* **2021**, *36*, 6662–6673. [CrossRef]
2. Deshmukh, S.; Iqbal, A.; Islam, S.; Khan, I.; Marzband, M.; Rahman, S.; Al-Wahedi, A.M.A.B. Review on classification of resonant converters for electric vehicle application. *Energy Rep.* **2022**, *8*, 1091–1113. [CrossRef]
3. Narasipuram, R.P.; Mopidevi, S.; Dianov, A.; Tandon, A.S. Analysis of Scalable Resonant DC–DC Converter using GaN switches for xEV Charging Stations. *World Electr. Veh. J.* **2024**, *15*, 218. [CrossRef]

4. Kheraluwala, M.H.; Gasgoigne, R.W.; Divan, D.M.; Bauman, E. Performance characterization of a high power dual active bridge DC/DC converter. In Proceedings of the Conference Record of the 1990 IEEE Industry Applications Society Annual Meeting, Seattle, WA, USA, 7–12 October 1990; pp. 3920–3924.
5. Hou, N.; Li, Y.W. Overview and comparison of modulation and control strategies for a nonresonant single-phase dual-active-bridge DC–DC converter. *IEEE Trans. Power Electron.* **2019**, *35*, 3148–3172. [CrossRef]
6. Shao, S.; Chen, H.; Wu, X.; Zhang, J.; Sheng, K. Circulating current and ZVS-on of a dual active bridge DC–DC converter: A review. *IEEE Access* **2019**, *7*, 50561–50572. [CrossRef]
7. De Doncker, R.W.A.A.; Divan, D.M.; Kheraluwala, M.H. A three-phase soft-switched high-power-density DC/DC converter for high-power applications. *IEEE Trans. Ind. Appl.* **1991**, *27*, 63–73. [CrossRef]
8. Zhao, B.; Yu, Q.; Sun, W. Extended-phase-shift control of isolated bidirectional DC–DC converter for power distribution in microgrid. *IEEE Trans. Power Electron.* **2011**, *27*, 4667–4680. [CrossRef]
9. Shi, H.; Wen, H.; Chen, J.; Hu, Y.; Jiang, L.; Chen, G.; Ma, J.Minimum-backflow-power scheme of DAB-based solid-state transformer with extended-phase-shift control. *IEEE Trans. Ind. Appl.* **2018**, *54*, 3483–3496. [CrossRef]
10. An, F.; Song, W.; Yang, K.; Luo, S.; Feng, X. Optimised power control and balance scheme for the output parallel dual-active-bridge DC–DC converters in power electronic traction transformer. *IET Power Electron.* **2019**, *12*, 2295–2303. [CrossRef]
11. Zhao, B.; Song, Q.; Liu, W.; Sun, W. Current-stress-optimized switching strategy of isolated bidirectional DC–DC converter with dual-phaseshift control. *IEEE Trans. Ind. Electron.* **2013**, *60*, 4458–4467. [CrossRef]
12. Zhao, B.; Song, Q.; Liu, W. Efficiency characterization and optimization of isolated bidirectional DC–DC converter based on dualphase-shift control for DC distribution application. *IEEE Trans. Power Electron.* **2013**, *28*, 1711–1727. [CrossRef]
13. Wen, H.; Su, B. Reactive power and soft-switching capability analysis of dual-active-bridge DC–DC converters with dual-phase-shift control. *J. Power Electron.* **2015**, *15*, 18–30. [CrossRef]
14. Hou, N.; Song, W.; Wu, M. Minimum-current-stress scheme of dual active bridge DC–DC converter with unified phase-shift control. *IEEE Trans. Power Electron.* **2016**, *31*, 8552–8561. [CrossRef]
15. Noroozi, N.; Emadi, A.; Narimani, M. Performance evaluation of modulation techniques in single-phase dual active bridge converters. *IEEE Open J. Ind. Electron. Soc.* **2021**, *2*, 410–427. [CrossRef]
16. Li, Z.; Li, M.; Zhao, Y.; Wang, Z.; Yu, D.; Xu, R. An Optimized Control Method of Soft-Switching and No Backflow Power for LLC Resonant-Type Dual-Active-Bridge DC-DC Converters. *Mathematics* **2023**, *11*, 287. [CrossRef]
17. Chen, L.; Lin, L.; Shao, S.; Gao, F.; Wang, Z.; Wheeler, P.W.; Dragicevic, T. Moving discretized control set model-predictive control for dual-active bridge with the triple-phase shift. *IEEE Trans. Power Electron.* **2020**, *35*, 8624–8637. [CrossRef]
18. Shao, S.; Jiang, M.; Ye, W.; Li, Y.; Zhang, J.; Sheng, K. Optimal phase-shift control to minimize reactive power for a dual active bridge DC–DC converter. *IEEE Trans. Power Electron.* **2019**, *34*, 10193–10205. [CrossRef]
19. Xu, F.; Liu, J.; Dong, Z. Minimum backflow power and ZVS design for dual-active-bridge DC–DC converters. *IEEE Trans. Ind. Electron.* **2022**, *70*, 474–484. [CrossRef]
20. Das, D.; Basu, K. Optimal design of a dual-active-bridge DC–DC converter. *IEEE Trans. Ind. Electron.* **2021**, *68*, 12034–12045. [CrossRef]
21. Bez, F.; Scandola, L.; Corradini, L.; Saggini, S.; Spiazzi, G. Twodimensional online efficiency optimization technique for dual active bridge converters. In Proceedings of the IEEE 17th Workshop on Control and Modeling for Power Electronics (COMPEL), Trondheim, Norway, 27–30 June 2016; pp. 1–8. [CrossRef]
22. Bhattacharjee, A.K.; Batarseh, I. Optimum hybrid modulation for improvement of efficiency over wide operating range for triplephase-shift dual-active-bridge converter. *IEEE Trans. Power Electron.* **2020**, *35*, 4804–4818. [CrossRef]
23. Li, X.; Zhang, X.; Lin, F.; Sun, C.; Mao, K. Artificial-intelligencebased triple phase shift modulation for dual active bridge converter with minimized current stress. *IEEE J. Emerg. Sel. Top. Power Electron.* **2023**, *11*, 4430–4441. [CrossRef]
24. An, F.; Song, W.; Yang, K.; Hou, N.; Ma, J. Improved dynamic performance of dual active bridge DC–DC converters using MPC scheme. *IET Power Electron.* **2018**, *11*, 1756–1765. [CrossRef]
25. Samad, T.; Bauer, M.; Bortoff, S.; Di Cairano, S.; Fagiano, L.; Odgaard, P.F.; Rhinehart, R.R.; Sánchez-Peña, R.; Serbezov, A.; Ankersen, F.; et al. Industry engagement with control research: Perspective and messages. *Annu. Rev. Control.* **2020**, *49*, 1–14. [CrossRef]
26. Song, C.; Sangwongwanich, A.; Yang, Y.; Blaabjerg, F. A modelfree capacitor voltage balancing method for multilevel DAB converters. *IEEE Trans. Power Electron.* **2023**, *38*, 79–84. [CrossRef]
27. Shao, S.; Chen, L.; Shan, Z.; Gao, F.; Chen, H.; Sha, D.; Dragičević, T. Modeling and advanced control of dual-active-bridge DC–DC converters: A review. *IEEE Trans. Power Electron.* **2022**, *37*, 1524–1547. [CrossRef]
28. An, F.; Song, W.; Yu, B.; Yang, K. Model predictive control with power self-balancing of the output parallel DAB DC–DC converters in power electronic traction transformer. *IEEE J. Emerg. Sel. Top. Power Electron.* **2018**, *6*, 1806–1818. [CrossRef]
29. Meng, X.; Jia, Y.; Xu, Q.; Ren, C.; Han, X.; Wang, P. A novel intelligent nonlinear controller for dual active bridge converter with constant power loads. *IEEE Trans. Ind. Electron.* **2023**, *70*, 2887–2896. 10.1109/TIE.2022.3170608. [CrossRef]
30. Jeung, Y.-C.; Lee, D.-C. Voltage and current regulations of bidirectional isolated dual-active-bridge DC–DC converters based on a doubleintegral sliding mode control. *IEEE Trans. Power Electron.* **2019**, *34*, 6937–6946. [CrossRef]
31. Lee, S.; Jeung, Y.-C.; Lee, D.-C. Voltage balancing control of IPOS modular dual active bridge DC/DC converters based on hierarchical sliding mode control. *IEEE Access* **2019**, *7*, 9989–9997. [CrossRef]

32. Tiwary, N.; Panda, A.K.; Lenka, R.K.; Narendra, A. Super twisting sliding mode control of dual active bridge DC–DC converter. In Proceedings of the IEEE International Conference on Power Electronics, Drives and Energy Systems (PEDES), Jaipur, India, 16–19 December 2020; pp. 1–5. [CrossRef]
33. Bagheri, F.; Guler, N.; Komurcugil, H. Sliding mode current observer for a bidirectional dual active bridge converter. In Proceedings of the 47th Annual Conference of the IEEE Industrial Electronics Society, Toronto, ON, Canada, 13–16 October 2021; pp. 1–6. [CrossRef]
34. Abdelkarim, E.; Kadi, S. Super twisted sliding mode control of isolated bidirectional DC–DC converter in electric vehicle. In Proceedings of the 22nd International Middle East Power Systems Conference (MEPCON), Assiut, Egypt, 14–16 December 2021; pp. 389–394. [CrossRef]
35. Tiwary, N.; Naik, V.R.N.; Panda, A.K.; Lenka, R.K.; Narendra, A. Sliding mode and current observer-based direct power control of dual active bridge converter with constant power load. *Int. Trans. Electr. Energy Syst.* **2021**, *31*, e12879. [CrossRef]
36. Ullah, N.; Farooq, Z.; Zaman, T.; Sami, I.; Ibeas, A.; Techato, K.; Chowdhury, S.; Muyeen, S. A computationally efficient robust voltage control for a single phase dual active bridge. *Energy Rep.* **2020**, *6*, 3346–3356. [CrossRef]
37. Deng, L.; Zhou, G.; Bi, Q.; Xu, N. Online reactive power minimization and soft switching algorithm for triple-phase-shift modulated dual active bridge converter. *IEEE Trans. Ind. Electron.* **2023**, *70*, 2543–2555. [CrossRef]